Textures and Microstructures, 1996, Vol. 26–27, pp. 11–18
Reprints available directly from the publisher.
Photocopying permitted by license only

MULTIPLE POLE FIGURE EXTRACTION FROM PULSED WHITE BEAM ANGLE-DISPERSIVE NEUTRON DIFFRACTION DATA

E. JANSEN[1], W. SCHÄFER[1], W. KOCKELMANN[1,2] and G. WILL[1]

[1]*Mineralogisches Institut der Universität Bonn, D-53115 Bonn, Germany*
[2]*and ISIS-Facility, Rutherford-Appelton-Laboratory, Chilton, OX11 0QX, U.K.*

(Received 17 January 1996)

The continuous wavelength spectrum available at pulsed neutron sources and the use of a position-sensitive detector can drastically reduce the number of sample orientations during pole figure scanning compared to the conventional method using monochromatic neutrons. This advantage has to be paid for by a more complex way in extracting pole figures from the measured data. The paper describes the experimental setup, the scanning procedure and the data evaluation of neutron diffraction texture measurements at a spallation source. A multitude of individual pole figures can be measured simultaneously within a reasonable time. The paper focuses on strategy and practical management to obtain pole figures from two-dimensional time-of-flight diffraction patterns.

KEY WORDS: Multiple pole figures, pulsed beam neutrons, angle-dispersive texture measuring techniques.

INTRODUCTION

Neutron diffraction is an attractive tool in texture analysis for several reasons. The high penetration capability of neutrons, which exceeds that of X-rays by about four orders of magnitude, allows the measurement of volume textures and to investigate irregular shaped specimens, thus meeting especially application aspects in earth sciences (Bunge *et al.*, 1994). Neutron diffraction and large neutron beam cross sections stand for high grain statistics even in the case of coarse grained geological specimens (Wenk *et al.*, 1984). Complete pole figures can be measured in transmission geometry; absorption corrections are mostly negligible. There are no angle dependent defocusing effects as known from X-ray pole figure scanning. Conventional monochromatic beam neutron texture diffractometers are nowadays equipped with large position-sensitive detectors (PSDs) for the simultaneous measurement of several pole figures (Will *et al.*, 1989). The so-called blind spot arising in pole figures from reflections measured at the outer parts of the PSD, can be overcome by a few additional measuring points (Bunge *et al.*, 1984). The advantages of using PSDs and applying peak deconvolution methods for the texture analysis of multiphase and low-symmetry materials have been discussed elsewhere (Wenk *et al.*, 1986, Merz, 1991, Schäfer *et al.*, 1991).

Nevertheless, people often hesitate to use neutron diffraction in texture investigations, especially at studies where large series of many individual samples are involved. That's mainly because of the high amount of expensive neutron beam time needed for pole figure scanning, apart from the worldwide poor availability of neutron instruments. Long

measuring times, exceeding those with X-rays by more than one order of magnitude, are necessary because of the rather poor monochromatic neutron flux at a steady state reactor. Essential reductions of neutron diffraction measuring times, however, can be achieved at pulsed neutron sources, where the complete thermal neutron spectrum can be exploited simultaneously by applying time-of-flight techniques (Schäfer *et al.*, 1993). The installation of high performance linear PSDs, capable of high resolution data collection with respect to both position (= Bragg angle) and time (= wavelength), allows short measuring times to accumulate d-spacing patterns (Schäfer *et al.*, 1995a).

PULSED SOURCE INSTRUMENTATION

The first dedicated neutron texture diffractometer to use the advantages of white beam time-of-flight techniques was built at the high flux pulsed reactor IBR-2 at Dubna (Feldmann, 1986). This instrument is equipped with several counting tubes at flexible Bragg-positions to register a certain number of pole figure points each. Several but incomplete pole figures are obtained simultanously by combining the individual counting tube data. The NSWR instrument at Dubna is being extended by the rearrangement of a large number of counting tubes around a Debye-Scherrer cone at $2\Theta = 90°$ (Heinitz *et al.*, 1995). Early texture measurements performed at a pulsed spallation source were reported from the Los Alamos Neutron Scattering Center using the two-dimensional area detector installation at the single crystal diffractometer SCD (Wenk *et al.*, 1988).

Very recently, our institute started the operation of a pulsed white beam angle-dispersive time-of-flight diffractometer at the ISIS spallation source (Schäfer *et al.*, 1995a). This instrument is equipped with two units of the linear JULIOS PSD of about 70 cm sensitive length each (Figure 1), which can be flexibly positioned at different angles and at variable distances from about 40 cm to 150 cm to the sample. The angle covered by one detector unit at minimum distance is about 90°. The JULIOS scintillation detector, which oringinally has been developed for spallation source instrumentation, is characterized by a neutron sensitivity of 65, 85 and 95% for neutrons of 1, 2 and 3Å wavelength, respectively. The linear spatial resolution is 2.3 mm; the time resolution of the JULIOS electronics is better than 1 μs (Schäfer *et al.*, 1994).

The instrument ROT/DIFF, which uses the wavelength band from 0.4Å to 4.2Å simultaneously, can be operated as dedicated texture diffractometer (see Schäfer *et al.*, 1995b, Jansen *et al.*, 1995). The main component besides the linear detector units is

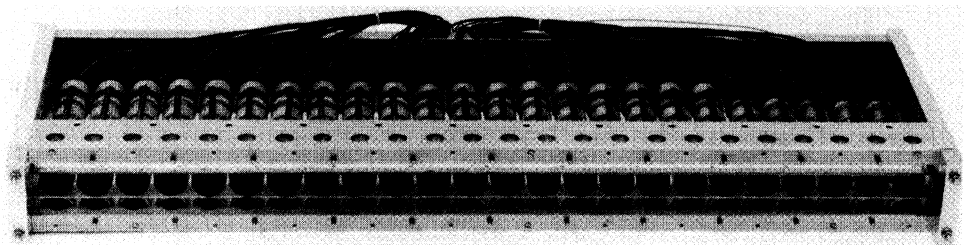

Figure 1 The scintillation detector JULIOS which consists of a linear array of photomultipliers with a ^{6}Li-glass scintillator in front of it.

a one-circle sample goniometer with a horizontal 360°-rotation axis driven by a stepping motor. The sample is mounted at the end of the rotation axis to be aligned in the center of the primary white neutron beam. The goniometer device itself is mounted on a turn-table allowing different orientations of the goniometer-axis with respect to the primary beam.

WHITE BEAM POLE FIGURE SCANNING

In a conventional set-up pole figures are measured in nested scans, a χ-scan running over the pole distances χ between 0 and 90° and a φ-scan at each χ-setting to cover the full circles of latitude. To get a complete pole figure, hundreds of sample orientations must be measured. Using a polychromatic beam and a linear detector, Bragg reflection conditions are fulfilled for different wavelengths at different positions of the detector. Thus, the reflection of a given {hkl} can appear along the total length of the detector due to the wavelength dependent scattering-angle, and different orientations of one Bragg plane can be seen simultaneously at different positions of the PSD (Figure 2). Because of this, it is possible to replace a scan, necessary at a conventional constant-wavelength diffractometer, by the angular extension of a PSD. Thus, pole figure scanning can be reduced to one or to a few φ-scans. In case of random crystallite orientations, there will be a continuous monotonic {hkl} intensity distribution along the detector; in case of a texturized sample, there will be a preferred orientation specific intensity variation as shown in Figure 3, obtained from recristallized copper (Engler *et al.*, 1993).

The angular spread of different crystallite orientations to be registered simultaneously depends on the scattering-angle covered by the detector. With a 180° detector, the total pole distance coverage of one hemisphere ($\Delta\chi$ = 90°) can be realized by one fixed turn table setting. The setting angle of the turn table is called the χ_0 setting because it determines the origin of the detectors χ-coverage. One should keep in mind, that in the geometry of Figure 2 the axis of the χ-rotation coincides with the turn table axis, usually called the ω-axis. For a complete pole figure, several χ_0-settings realized

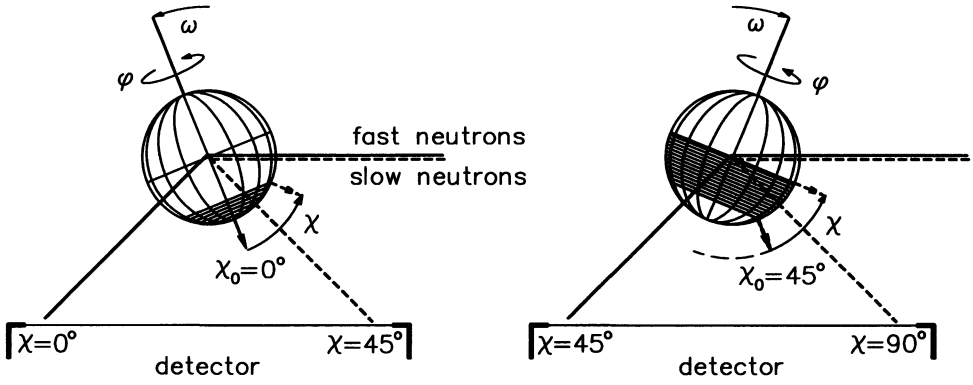

Figure 2 The pole projection sphere in two different χ_0-settings. *Left:* Fast neutrons reflected by Bragg planes perpendicular to χ = 0° reach the left part of the detector, slow ones reflected from Bragg planes of the same d-spacing but perpendicular to χ = 45° reach on the right side. *Right:* Different χ_0-setting results in the reflection of different oriented planes.

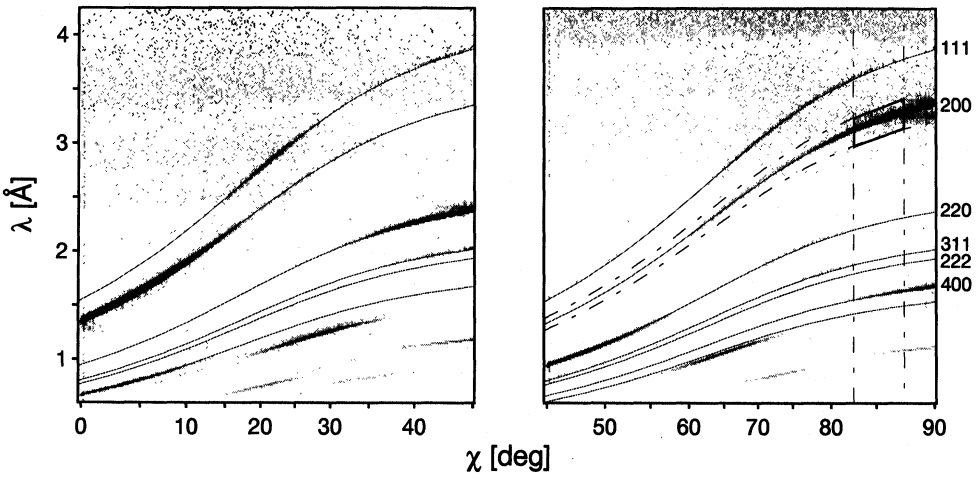

Figure 3 Two-dimensional spectra of copper, taken at $\varphi = 0°$ and the two χ_0-settings of Figure 2. Darker gray stands for higher intensity. The curved lines are the traces of d-spacing belonging to the Bragg plane indicated on the right.

by using the ω-rotation mechanics are necessary in case of detectors with smaller angular coverage, e.g. two different χ_0-settings for a 90°-detector (see Figure 2). The grid of sample orientations for the pole figure scanning is defined in a file, which can be edited to meet the requirements of the desired pole figure resolution. In total, the white beam pole figure scanning pattern is obtained by roughly 1/10 of the sample orientations needed in the conventional χ / φ scanning mode with monochromatic neutrons.

It should be stated that the combination of white beam time-of-flight technique and the use of a linear detector meets two objectives simultaneously:

(1) the reduction of sample orientations in the course of pole figure scanning and

(2) the simultaneous measurement of a multitude of different {hkl} pole figures.

In constant-λ diffraction the linear detector can achieve this only alternatively: either (1), when installed vertically at $2\Theta = 90°$ (Jensen, *et al.*, 1983) or (2) when installed in the horizontal scattering plane of the diffractometer (Schäfer *et al.*, 1991). Obviously, the new technique of angle dispersive time-of-flight pole figure data collection leads to a rather sophisticated procedure in data processing and analysis. The following discussion will be confined to the case of a 90°-detector and focuses on the copper sample mentioned above.

POLE FIGURE DATA PROCESSING AND EVALUATION

In the course of the measurement with two χ_0-settings and an azimuth step width of $\Delta\varphi = 7.2°$ at the larger and $\Delta\varphi = 10°$ at the smaller pole-distances – different stepsizes are due to the different extents of the circles of latitude – a total of 86 different datasets is obtained. Figure 4 shows the projections of the PSD during the pole figure scan.

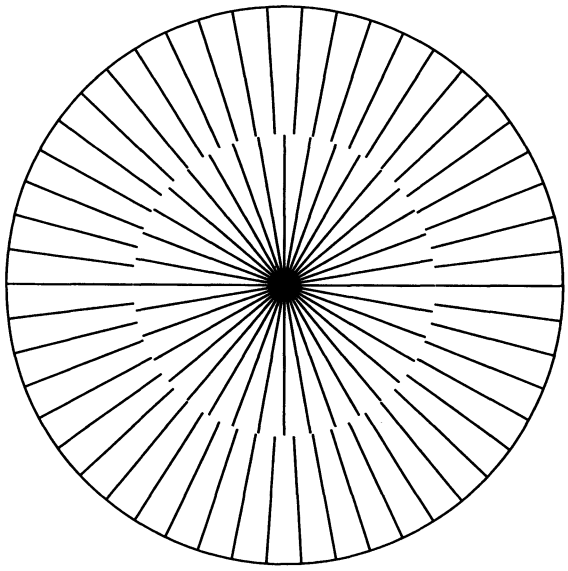

Figure 4 Traces of the detector on the pole projection sphere during the χ_0 / φ-scan (equal area projection).

Each dataset is identified by an unique name made up of the χ_0 / φ-setting. It contains a data point matrix of 2^{r+c} count rates ordered in r rows of equispaced time-of-flight channels and in c columns belonging to different detector-positions; actually, $r = c = 8$ gives a 256 by 256 data point matrix. Each time channel corresponds to a wavelength λ according to de Broglie's law. The position channels correspond to scattering angles and simultaneously to pole distances according to the scattering geometry explained above. The straight-forward strategy to extract pole figures from the 86 datasets is as follows.

(1) *Correction for channel-sensivity and primary beam intensity:* In a first step, all the two-dimensional spectra are corrected according to the position dependent channel sensitivity and the time dependent primary beam intensity. To carry out the sensitivity correction, a row vector containing factors for all columns is calculated from a comparative measurement with a homogeneously scattering sample, usually a vanadium rod. An equivalent column vector is obtained from a time dependent monitor spectrum. The correction is carried out by multiplying each data point with the factors corresponding to the point's row and column.

(2) *Background separation:* Subsequently, the background is separated from the spectra. For this, a mean spectrum is calculated by accumulating and averaging all spectra. In this mean spectrum, a grid of background points is determined in a graphic interactive environment (Jansen *et al.*, 1993) with the help of constant time and constant position sections through the mean spectrum. An interpolation surface through the grid points gives the mean background to be substracted from the individual spectra. The spectra of Figure 3 were obtained at this stage.

(3) *Geometrical Lorentz correction:* The next point in the course is the Lorentz correction of the data points dependent on scattering angle and wavelength. As in the sensitivity/ intensity correction, first row and column vectors are calculated to be subsequently multiplied into all data point matrices.

(4) *Selection of d-spacing limits of individual pole figures:* To extract an individual pole figure one needs limiting d-values, between which the measured intensities can contribute to a selected Bragg reflection. As an aid, the two-dimensional mean spectrum is focussed into a one-dimensional equi-spaced $\Delta d/d$ spectrum by averaging all intensities belonging to the same $\Delta d/d$ channel, obeying the appropriate Lorentz correction. In this $\Delta d/d$ spectrum, shown in Figure 5, the limiting d-values can be easily determined. The resulting traces of these limits around the Bragg peak marked in Figure 5 are shown in Figure 3 as dashed lines above and below the trace of the peak maximum.

(5) *Selection of the pole distance stepwidth:* At this stage, one has a nearly continuous spectrum of χ-counts, and therefore one can decide, which χ-stepwidth should be simulated. The limits resulting from a width of 5° around a central χ appear as fine vertical lines in Figure 3.

(6) *Getting the count of a given χ / φ-setting:* For instance, to get the count belonging to the central $\chi = 85°$ one has to integrate all counts of the area within the box between the limiting lines in Figure 3. This figure represents the data measured at $\varphi = 0°$ and therefore this integral is equivalent to a count measured in the conventional monochromatic way at $\chi = 85°$ and $\varphi = 0°$ in the appropriate 2Θ-setting for the marked peak. Using all positions and all reflection traces of all diagrams, one gets raw data grids for a multitude of pole figures comparable to those obtained in a conventional way.

(7) *Obtaining a pole figure:* The further procedure is equivalent to the common practice to generate an equispaced grid using spline methods followed by a normalization considering the different extents of the χ-circles to get a χ / φ-matrix of pole densities,

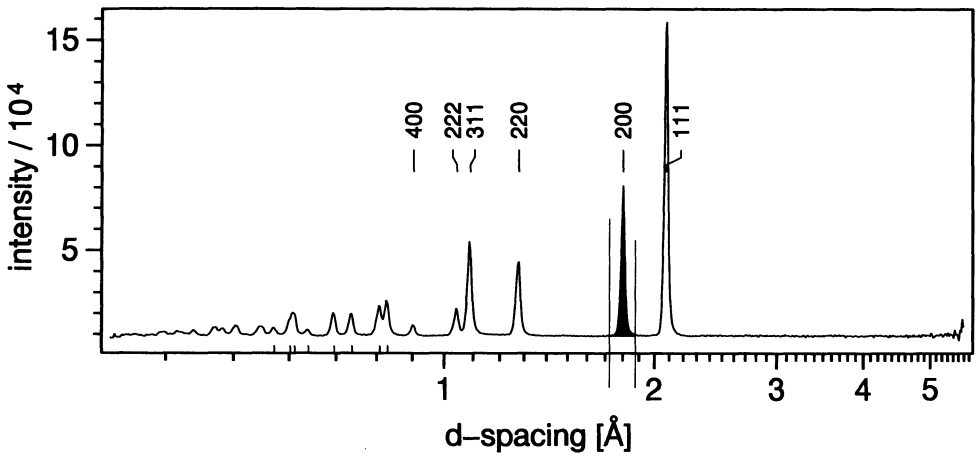

Figure 5 d-spacing pattern of copper, obtained from the mean of all two-dimensional spectra, taken at all χ_0/ φ-orientations. Around the (200)-reflection d-limits are marked, between which counts can contribute. The measurements were performed with a detector distance of 36 cm from the sample.

that may be plotted or processed in subsequent routines resulting into the orientation distribution function.

Figure 6 shows the {200} pole figure of the copper sample, one of six pole figures registered simultaneously. Small rectangles mark the projections of the PSD during the observation of the data of Figure 3.

CONCLUSIONS

The new method was tested on various samples. Some problems occured at weak texturized samples because of insuffient primary beam monitoring during the first test measurements, but in the meantime a permanent monitor system has been installed to overcome uncertainties in primary beam intensity.

The measuring time for one χ / φ-setting was 40–100 s, resulting in a total time about 1h up to 2.5h for all the 86 orientations, and the time for the extraction procedure is of the same order of magnitude using a modern Personal Computer. In general, one scanning procedure yields enough independent pole figure to obtain the orientation distribution function.

Acknowledgements

The authors would like to acknowledge the financial support by the Bundesminister für Bildung, Wissenschaft, Forschung und Technologie, Bonn, under the contract Nos. WI4BO2 and WI4BO3.

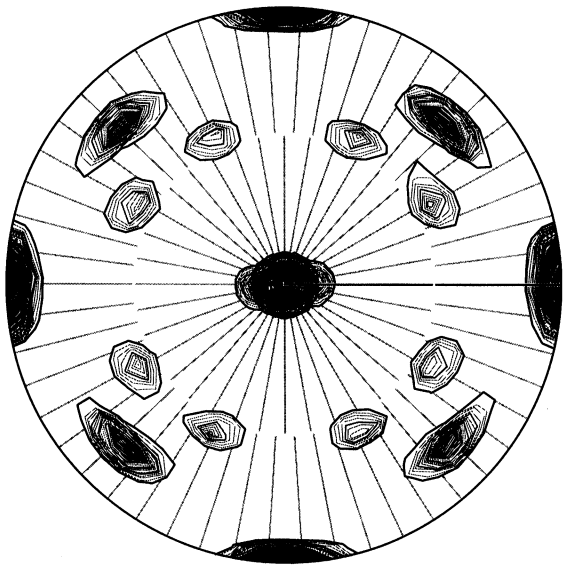

Figure 6 Equal area projection of the {200} pole figure of recristallized copper. The bold radial lines indicate the χ_0 / φ-settings during the collection of the data sets shown in Figure 3.

References

Bunge, H. J., Wenk, H.-R. and Pannetier, J. (1984). *Textures and Microstructures*, **5**, 153–170.
Bunge, H. J., Siegesmund, S., Skotzki, W. and Weber, K., eds. (1994). *Textures of Geological Materials*, DGM Informationsgesellschaft Verlag, Oberursel.
Engler, O., Palacios, J., Schäfer, W., Jansen, E., Lücke, K. and Will, G. (1993). *Textures and Microstructures*, **21**, 195–206.
Feldmann, K. (1986). in *Experimental Techniques of Texture Analysis* (ed. Bunge, H. J.), DGM Informationsgesellschaft Verlag Oberursel, pp. 253–263.
Heinitz, J., Isakov, N. N. and Walther, K. (1995). *Deutsche Neutronenstreutagung '95, Reinstorf/ Lüneburg*.
Jansen, E., Schäfer, W. and Will, G. (1993). *Proc. of EPDIC-III, Material Science Forum*, **166–169**, 187–192.
Jansen, E., Schäfer, W., Will, G. and Knight, K. S. (1995). *Proc. of EPDIC-IV, Materials Science Forum*, in print.
Jensen, D. J. and Kjems, J. K. (1983). *Textures and Microstructures*, **5**, 239.
Merz, P. (1991). *KFA-Report Jül-2443*, Forschungszentrum Jülich.
Schäfer, W., Merz, P., Jansen, E. and Will, G. (1991). *Textures and Microstructures*, **14–18**, 65–71.
Schäfer, W., Jansen, E. and Will, G. (1993). *J. Appl. Cryst.*, **26**, 660–669.
Schäfer, W., Jansen, E., Szepesvàry, A., Skowronek, R., Will, G., Reinartz, R. and Müller, K. D. (1993). *Proc. of ICANS-XII, RAL-Report*, **94–025** pp. 1200–1207.
Schäfer, W., Jansen, E., Skowronek, R., Will, G., Kockelmann, W., Schmidt, W. and Tietze-Jaensch, H. (1995). *Nucl. Instrum. Methods in Phys. Research*, **A364**, 179–185.
Schäfer, W., Jansen, E., Kockelmann, W., Tietze-Jaensch, H. and Will, G. (1995a). *Proc. of ICANS-XIII*, PSI, Villigen Switzerland, in print.
Wenk, H.-R., Kern, H., Schäfer, W. and Will, G. (1984). *J. Structural Geology*, **6**, 687–692.
Wenk, H.-R., Bunge, H. J., Pannetier, J. and Jansen, E. (1986). *Tectonophysics*, **126**, 271–284.
Wenk, H.-R., Vergamini, P. J. and Larson, A. C. (1988). *Textures and Microstructures*, **10**, 443.
Will, G., Schäfer, W. and Merz, P. (1989). *Textures and Microstructures*, **10**, 375–387.